Biointerface Research in Applied Chemistry
Open-Access Journal (ISSN: 2069-5837)

Article
Volume 16, Issue 1, 2026, 8
https://doi.org/10.33263/BRIAC161.008

Characterization and Functionalization of Diabetes Medication (BNEJa): A Step Forward in Nano Drug Delivery System

Fatemeh Mollaamin [1,*], Majid Monajjemi [2]

[1] Department of Biomedical Engineering, Faculty of Engineering and Architecture, Kastamonu University, Kastamonu, Turkey
[2] Department of Biology, Faculty of Science, Kastamonu University, Kastamonu, Turkey
* Correspondence: fmollaamin@kastamonu.edu.tr;

Received: 28.10.2025; Accepted: 17.12.2025; Published: 15.02.2025

Abstract: In this research, the interaction between the anti-diabetic drug of (BNEJa) and armchair single-walled carbon nanotube (SWCNT) has been calculated with density functional theory (DFT) to ameliorate carbon nanotube drug carriers as the applied sensors in drug delivery systems. BNEJa shows NMR shielding between 10–600 ppm, with a sharp peak at 25 ppm and several weak peaks between 100–450 ppm. The hydrogens involved in the O–H of PO_3 groups have remarked the high degeneracy in NMR chemical shielding tensors. The largest fluctuation in atomic charge has been observed for the oxygen atoms in the O–H of PO_3 groups, as the electronegative atoms in the formation of potent chelation with the carbon nanotube using the drug delivery method, suggesting the modeling of (BNEJa)@SWCNT. Moreover, the electric potential (Ep) as the amount of work energy through transferring the electric charge from one site to another site in the presence of an electric field has been measured for blood pressure (BP) agent of (BNEJa) @ SWCNT complex using CAM–B3LYP/EPR–III, 6–311+G(d,p) level of theory. So, the electric potential of the NQR method for elements of N, P, O, and F, dealing with the interaction site between the BP agent of (BNEJa) and the surface of SWCNT in aqueous medium. The parameter values have shown good stability of the BP agent during Langmuir adsorption on the SWCNT sensor.

Keywords: diabetes medication; SWCNT sensor; drug delivery; computational method.

1. Introduction

Although the aetiologies of type 1 and type 2 diabetes vary extremely, both cause hyperglycaemic states, and both exhibit common macrovascular complications, such as cerebrovascular, coronary heart, and peripheral vascular disease, and microvascular complications like neuropathy, nephropathy, and retinopathy [1-4].

Phosphoeleganin was shown to inhibit both enzymes, acting as a pure non-competitive inhibitor of PTP1B and a mixed-type inhibitor of AR. Furthermore, in silico docking analyses to estimate the interaction mode of phosphoeleganin with both enzymes were done [3-6]. The inhibitory mechanisms on protein tyrosine phosphatase 1B (PTP1B) and aldose reductase (AR) enzymes, including analysis of the insulin signalling pathway of phosphoeleganin, were investigated [7-11].

Since the exploration of CNTs in the 1990s and the advancement of their application in nanomedicine, these compounds have become significant due to their properties, including rich electronic and thermal properties, high mechanical strength, high chemical stability, and extremely low weight [12]. These carriers enable the transfer of therapeutic agents, such as proteins, DNA, antibodies, and drugs, either through the external wall or by trapping them in the nanotubes' cavities as capsules [13].

Nanotubes with their intrinsic properties have been considered potential candidates for drug delivery carriers. The capped ends of nanotubes may be opened up by oxidation, allowing for the insertion of molecules of interest inside the nanotube. Carbon nanotubes (CNTs) can easily penetrate cells, delivering drugs directly to the cytoplasm or nucleus [14].

CNTs are long and tubular fullerene structures, which can be either single-walled (SWCNTs) or multi-walled (MWCNTs) [15]. Nanotubes conform to a perpendicular position with the cell membrane during uptake, perforating and diffusing through the lipid bilayer to enter the cytoplasm. Functionalized CNTs are easily internalized by cells through passive and endocytosis-independent mechanisms [16].

In fact, the most popular bisphosphonate medications have a rich tension for metal cations, among them Ca^{2+}, with which they can produce both soluble and insoluble compounds and aggregates, depending on the pH of the solution and the metal concentration. The bisphosphonates are separated into chemical branches based on the side chains of R1 and R2. It is seen as a central carbon in bisphosphonates with two side chains of R1, R2, and two phosphate branches, which are bonded to Ca^{2+} through O- of PO_3 groups for keeping a high amount of Ca^{2+} in the bones of human body cells [17].

Non-N-containing bisphosphonates like clodronate, etidronate, and tiludronate are discussed as the first generation of bisphosphonates, which are simple molecules including single atoms or alkyl groups in side chains of R1 and R2, having a weak inhibitory impact on bone resorption [18].

Adding an amino group introduced starting the second generation of bisphosphonates, which were more powerful, such as pamidronate as the first one, and other identical compounds where the situation of the nitrogen in the side chain was the clue to a more efficient medication [19]. Currently, the third generation of bisphosphonates, including N-containing heterocyclic bisphosphonates like zoledronate and risedronate, has been presented and has displayed the strongest antiresorptive attributes [20,21].

This article aims to investigate the interaction between the anti-diabetic drug BNEJa and armchair single-walled carbon nanotubes (SWCNTs) based on DFT theory. The goal is to design, improve, and expand carbon nanotube drug carriers for use as sensors in drug delivery systems.

2. Materials and Methods

In this study, the geometries were optimized within the framework of DFT using the three-parameter Becke's exchange and Lee-Yang-Parr's correlation non-local functional, usually known as the–B3LYP method and basis set of 6–311+G(d,p)/EPR-III [22–24]. Then, the electronic structure of the adsorbed (5,5) armchair SWCNT by the bisphosphonate agent of (BNEJa) extracted from protein 1LQF was measured to measure physico-chemical properties. The density functional theory (DFT) is one of the most employed approximations of Hohenberg, Kohn, and Sham, which permits the theoretical study of material properties [25].

DFT theory proves an advantageous method for predicting chemical systems, and in order to understand its similarities and differences to other computational methods employed [26].

Development of the applied Density Functional Theory (DFT) methodology only became notable after W. Kohn and L. J. Sham released their reputable series of equations, which are introduced as Kohn-Sham (KS) equations [22,27]:

$$\hat{H}_s = -\sum_i^M \frac{1}{2} \overline{\nabla}_i^2 + \sum_i^M v_s(\vec{r}_i) = \sum_i^M \hat{h}_s \quad (1)$$

$$\hat{h}_s = -\frac{1}{2} \overline{\nabla}_i^2 + v_s(\vec{r}_i) \quad (2)$$

By representing the single particle orbitals ψ_i, all electronic densities physically acceptable for the system of "non-interacting" electrons are written in equation (3):

$$\rho(\vec{r}) = \sum_i^M |\psi_i(\vec{r})|^2 \quad (3)$$

Finally, the total energy could be measured by the KS method due to equation (4):

$$E[\rho] = \sum_i^M n_i \langle \psi_i \left| -\frac{1}{2} \overline{\nabla}^2 + v_{ext}(\vec{r}) + \frac{1}{2} \int \frac{\rho(\vec{r}')}{|\vec{r}-\vec{r}'|} d\vec{r}' \right| \psi_i \rangle + E_{xc}[\rho] + \frac{1}{2} \sum_\beta^N \sum_{\alpha \neq \beta}^N \frac{Z_\alpha Z_\beta}{|\vec{R}_\alpha - \vec{R}_\beta|} \quad (4)$$

Therefore, the precise exchange energy functional is described by the Kohn–Sham orbitals in lieu of the density, which is cited as the indirect density functional. This research has employed the penetration of the hybrid functional of three-parameter basis set of B3LYP (Becke, Lee, Yang, Parr)" within the conception of DFT upon theoretical computations and basis sets of LANL2DZ for alkali metal atoms and 6–311+G (d,p) for other atoms [23,24] with multiplicity of +1 and convergence on RMS density matrix=1.00D-08 and convergence on MAX density matrix=1.00D-06.

Furthermore, the Onsager model, which was developed by Frisch, Wong, and Wiberg, utilizes spherical cavities. Even though this implies a less accurate description of the solute-solvent interface, this approximation simplifies the evaluation of energy changes during geometry optimizations and frequency analyses. Moreover, Cramer and Truhlar improved this model at the dipole level [28]. In fact, a cavity must have a physical sense, as in the Onsager model, and a mathematical ability, as is often the case in other descriptions of solvent effects [28]. Specifically, the cavity has to keep out the solvent and include its frontiers as the biggest probability part of the solute charge distribution [28].

Then, the gauge including atomic orbitals (GIAO) has been adopted to solve the gauge problem in the calculation of nuclear magnetic shielding for the complex of (BNEJa) @ SWCNT using density functional theory (DFT) calculations by the Gaussian 16 revision C.01 program [21].

3. Results and Discussion

CNTs represent drug delivery platforms that can be functionalized with various biomolecules, including antibodies, proteins, and DNA. This permits the particular targeted for transferring the special tissues, organs, or cells. These compounds can easily penetrate cells,

delivering drugs directly to the cytoplasm or nucleus. Drug delivery systems improve the pharmacological and therapeutic profile and efficacy of the drug and lower the occurrence of off-targets based on previous investigations.

3.1. NMR analysis and charge distribution.

The computed results extracted from nuclear magnetic resonance (NMR) [29] have indicated the SCF GIAO magnetic shielding tensor in ppm for nitrogen, phosphorus, oxygen, and fluorine, exploring the active site of (BNEJa) as an anti-diabetic drug adsorbed on the (5,5) armchair SWCNT as the inhibitor of PTP-1B, suggested for the treatment of type 2 diabetes. The calculations have been accomplished based on CAM–B3LYP/6–311+G (d,p) level of theory using Gaussian 16 revision C.01 program [21] and have been reported in Table 1. The NMR data of isotropic (σ_{iso}) and anisotropic shielding tensor (σ_{aniso}) for (BNEJa) adsorbed on the SWCNT have been estimated (Table 1).

Table 1. SCF GIAO magnetic shielding tensor (σ_{iso} and σ_{aniso}), electric potential (E_p), and Charge distribution (Q) for (BNEJa) at the adsorption site onto SWCNT in aqueous medium.

Element	σ_{iso} (ppm)	σ_{aniso} (ppm)	E_p (a.u.)	Q (Coulomb)
O(2)	355.54	154.03	–22.31	–0.60
O(3)	162.13	85.58	–22.04	–0.24
O(4)	410.12	78.60	–22.03	–0.25
F(6)	468.18	60.39	–26.14	–0.16
F(7)	60.39	59.16	–26.14	–0.12
O(17)	81.53	842.88	–22.06	–0.29
N(18)	250.50	93.42	–18.07	–0.18
N(22)	256.93	96.15	–18.11	–0.02
O(23)	79.66	835.56	–22.10	–0.30
F(31)	463.14	61.41	–26.17	–0.16
F(32)	459.95	57.13	–26.17	–0.15
P(33)	601.40	234.55	–53.14	1.24
O(34)	416.05	85.13	–22.05	–0.25
O(35)	359.42	138.03	–22.33	–0.62
O(36)	394.59	79.11	–22.07	–0.25
N(37)	251.37	90.08	–18.06	–0.17
O(39)	71.57	831.66	–22.07	–0.30
O(44)	263.94	104.19	–21.98	–0.09
O(45)	111.60	837.71	–22.04	–0.27
N(46)	258.64	91.11	–18.08	–0.17
O(48)	110.32	917.71	–22.09	–0.30

In the aqueous medium, the agent of (BNEJa) adsorbed onto SWCNT has shown the fluctuation behavior for various atoms of nitrogen, phosphorus, oxygen, and fluorine in the active sites of this compound through the NMR chemical shielding tensor (Figure 1).

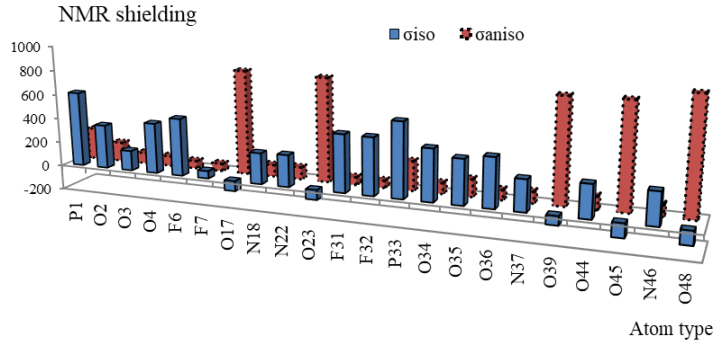

Figure 1. ^{13}C-NMR shielding (ppm) of isotropic (σ_{iso}) and anisotropic (σ_{aniso}) calculated for (BNEJa) using SCF GIAO method due to CAM–B3LYP function and 6–311+G(d,p) basis set through electronegative atoms of N, P, O, F as the active positions in the structures of an anti-diabetic drug.

The CS tensors have been yielded by the quantum chemical calculations in the principal axes system to estimate the isotropic chemical shielding (CSI), $(\sigma_{33}+ \sigma_{22} + \sigma_{11})/3$, and anisotropic chemical shielding (CSA), $\sigma_{33}-(\sigma_{22} + \sigma_{11})/2$ [29]. Besides, the Onsager model has influenced the nuclear magnetic resonance data and chemical shielding of H, C, N, O, P, and F atoms in (BNEJa) (Figure 2). The results of ^{1}H-NMR spectroscopy in Figure 2 have shown the fluctuation of chemical shielding using nuclear magnetic resonance for the bisphosphonate agent of (BNEJa) adsorbed on the SWCNT.

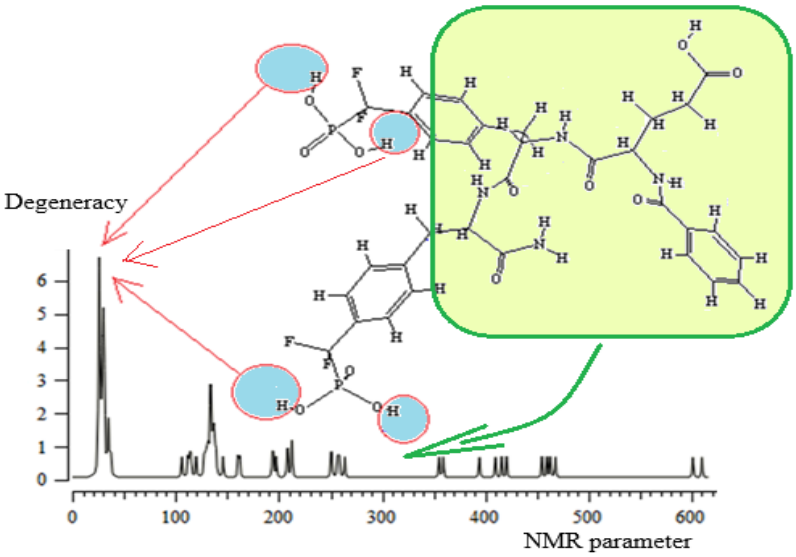

Figure 2. ^{1}H-NMR shielding (ppm) of (BNEJa) adsorbed on the SWCNT using SCF GIAO method due to B3LYP function and 6–311+G (d, p) basis set.

As a matter of fact, (BNEJa) has shown the NMR shielding between 10–600 ppm with a sharp peak at 25 ppm and several weak peaks between 100–450 ppm (Figure 2). The hydrogens involved in the O–H of PO_3 groups have remarked the high degeneracy in NMR chemical shielding tensors (Figure 2).

In the next step, the atomic charge of indicated atoms of N, P, O, and F in the junction of (BNEJa) with SWCNT has been evaluated (Table 1).

The results of Table 1 in a polar zone have declared the stability of (BNEJa) as an anti-diabetic drug, which has been modeled using the drug delivery method. The largest fluctuation in atomic charge has been seen for the oxygen atoms in O–H of PO_3 groups as the electronegative atoms in the formation of the potent chelation with carbon nanotube using the drug delivery method, which has suggested the modeling of (BNEJa) @ SWCNT (Figure 3).

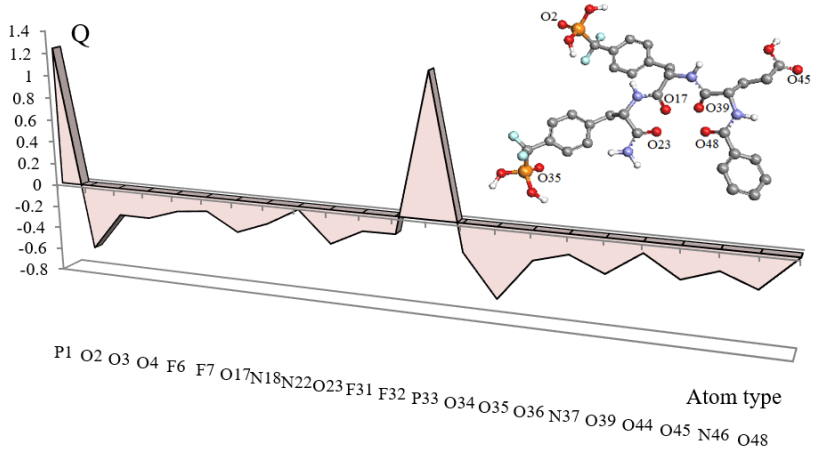

Figure 3. Changes of atomic charge (Q) for some electronegative atoms of N, P, O, and F in the active sites of (BNEJa) in the junction with SWCNT.

The perspective of Figure 3 recommends the reason for the existing observed various results of (BNEJa) @ SWCNT complex, which presents the position of active sites of labeled N, P, O, and F atoms in this chelation, which transfers the charge of electrons in the polar bisphosphonate agent of (BNEJa) toward (5,5) SWCNT.

3.2. NQR analysis.

As the EFG at the position of the nucleus in organic inhibitors is assigned by the valence electrons twisted in the special linkage with close nuclei of aluminum surface, the NQR [30] frequency at which transitions happen is particular for a BP agent of (BNEJa) @ SWCNT complex in aqueous medium (Table 1).

Therefore, the electric potential (E_p) (Table1) as the amount of work energy through transferring the electric charge from one site to another site in presence of electric field has been measured for BP agent of (BNEJa) @ SWCNT complex using CAM–B3LYP/EPR–III, 6–311+G(d,p) level of theory (Figure4). So, in Figure 4, the electric potential of the NQR method for elements of N, P, O, and F, dealing with the interaction site between the BP agent of (BNEJa) and the surface of SWCNT in aqueous medium.

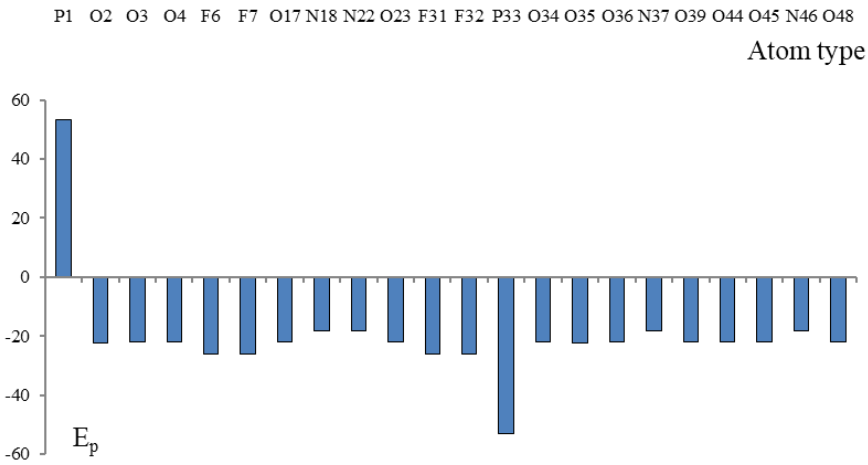

Figure 4. The changes of the electric potential versus atom type through NQR calculation for BP agent of (BNEJa) in the aqueous medium adsorbed on the SWCNT sensor by CAM–B3LYP/EPR–III, 6–311+G(d,p) calculation.

In NQR, nuclei with spin≥ 1, there is an electric quadrupole moment which is accompanied by non-spherical nuclear charge distributions. So, the nuclear charge distribution deviates from that of a sphere as the oblate or prolate form of the nucleus [30].

The NQR method is based on the multipole expansion in Cartesian coordinates as follows:

$$V(r) = V(0) + \left[\left(\frac{\partial V}{\partial x_i}\right)\Big|_0 . x_i\right] + \frac{1}{2}\left[\left(\frac{\partial^2 V}{\partial x_i x_j}\right)\Big|_0 . x_i x_j\right] \qquad (5)$$

Then, after simplification, the equation has only the second derivatives dependent on the same variable for the potential energy [30]:

$$U = -\frac{1}{2}\int_{\mathcal{D}} d^3\, r\, \rho_r \left[\left(\frac{\partial^2 V}{\partial x_i^2}\right)\Big|_0 . x_i^2\right] = -\frac{1}{2}\int_{\mathcal{D}} d^3\, r\, \rho_r \left[\left(\frac{\partial E_i}{\partial x_i}\right)\Big|_0 . x_i^2\right] = -\frac{1}{2}\left(\frac{\partial E_i}{\partial x_i}\right)\Big|_0 . \int_{\mathcal{D}} d^3\, r\, [\rho(r) . x_i^2] \qquad (6)$$

There are two parameters which must be obtained from NQR experiments: the quadrupole coupling constant, χ, and the asymmetry parameter of the EFG tensor, η:

$$\chi = {}^{e^2 Q q_{zz}}/_{h} \quad (7)$$

$$\eta = {}^{q_{xx} - q_{yy}}/_{q_{zz}} \quad (8)$$

Where q_{ii} are components of the EFG tensor at the quadrupole nucleus determined in the EFG principal axes system, Q is the nuclear quadrupole moment, e is the proton charge, and h is Planck's constant [30, 31].

It has been observed that the effects of N, P, O, and F in the BP agent (BNEJa) adsorbed to a (5,5) armchair SWCNT sensor were reflected in the electric potential measured by NQR analysis (Table 1). It's obvious that the graph of NQR characteristics for (BNEJa) @ SWCNT complex has the most fluctuation in the region of the two phosphorus of PO_3 groups (Figure 4).

3.3. Natural bond orbitals (NBO).

The Natural Bond Orbital (NBO) analysis [32] of (BNEJa) as an anti-diabetes has illustrated the character of electronic conjugation between bonds in the inhibitor and SWCNT sensor (Table 2 and Figure 5).

Table 2. NBO analysis for (BNEJa) as an anti-diabetes drug adsorbed on the SWCNT.

Bond orbital	Hybrids	Occupancy
BD1 P(1) –O(2)	0.6990 ($sp^{2.12}$) P + 0.7152 ($sp^{7.89}$) O	1.97
BD1 P(1) –O(3)	0.6033 ($sp^{3.28}$) P + 0.7975 ($sp^{5.71}$) O	1.97
BD1 P(1) – O(4)	0.6046 ($sp^{3.19}$) P + 0.7965 ($sp^{5.78}$) O	1.97
BD1 P(1) – C(5)	0.6686 ($sp^{3.83}$) P + 0.7436 ($sp^{3.44}$) C	1.93
BD1 O(3) – H(55)	0.7817 ($sp^{4.28}$) O + 0.6236 (σ) H	1.98
BD1 O(4) – H(56)	0.7808 ($sp^{4.27}$) O + 0.6248 (σ) H	1.98
BD1 C(5) – F(6)	0.6167 ($sp^{3.22}$) C + 0.7872 ($sp^{7.14}$) F	1.98
BD1 C(5) – F(7)	0.6268 ($sp^{2.94}$) C + 0.7792 ($sp^{7.45}$) F	1.99
BD1 C(15) – N(37)	0.6456 ($sp^{3.25}$) C + 0.7637 ($sp^{2.11}$) N	1.98
BD1 C(16) – O(17)	0.6563 ($sp^{1.86}$) C + 0.7545 ($sp^{3.42}$) O	1.99
BD1 C(16) – N(18)	0.6446 ($sp^{2.13}$) C + 0.7645 ($sp^{1.83}$) N	1.98
BD1 N(18) – C(19)	0.7691 ($sp^{2.13}$) N + 0.6391 ($sp^{3.28}$) C	1.98
BD1 C(21) – N(22)	0.6446 ($sp^{2.11}$) C + 0.7646 ($sp^{1.88}$) N	1.99
BD1 C(21) – O(23)	0.6538 ($sp^{1.92}$) C + 0.7567 ($sp^{3.32}$) O	1.99

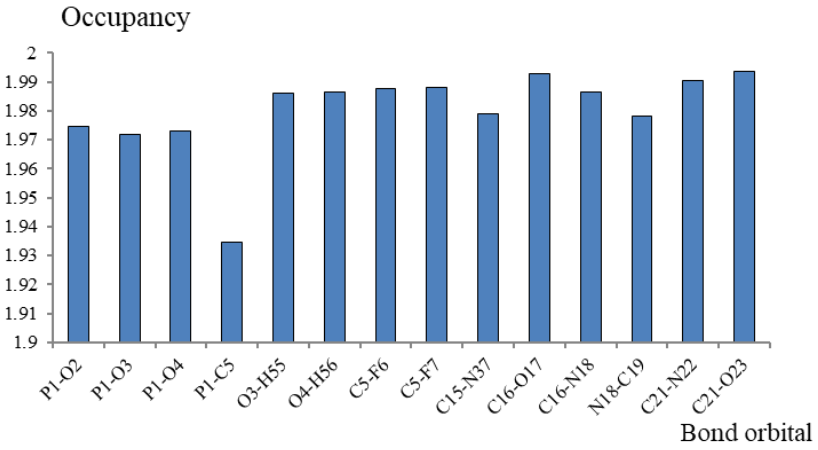

Figure 5. Occupancy fluctuation extracted from the NBO method for the (BNEJa) inhibitor adsorbed on the SWCNT.

In Figure 5, the fluctuation of occupancy of natural bond orbitals for (BNEJa) inhibitor adsorbed on SWCNT through bond orbitals containing P–O, O–H, C–F, C–N, C–O toward the Langmuir adsorption process by indicating the charge density from the heterocyclic compound of bisphosphonate agent close to the nanotube.

3.4. IR spectroscopy.

The infrared (IR) calculations have been accomplished for the BP agent of (BNEJa) in the aqueous medium adsorbed on the SWCNT by CAM–B3LYP/EPR–III, 6–311+G (d,p) level of theory to achieve the more accurate equilibrium geometrical parameters. Based on Figure 6, the IR spectrum analysis, the authors have concluded that this protective film consisted of an [(BNEJa) @ SWCNT] complex.

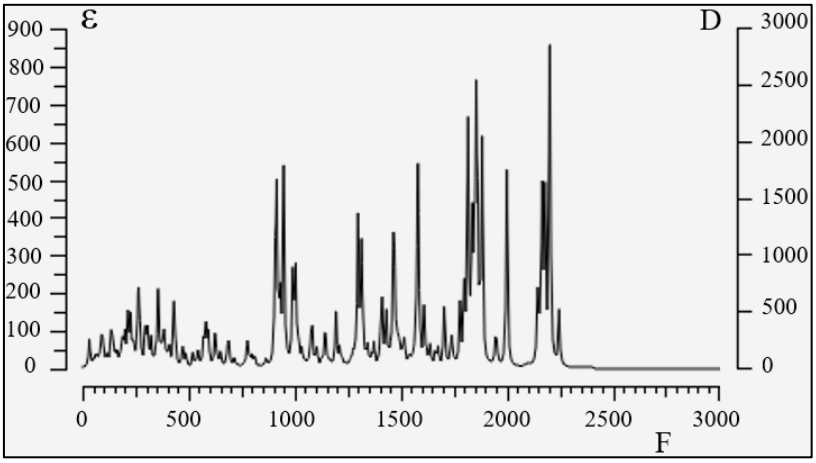

Figure 6. Diagram of IR spectra for BzN-EJJ-amid adsorbed on the surface of (5,5) armchair SWCNT using CAM–B3LYP/6–311+G(d,p) calculations. Note: F=frequency (cm^{-1}), ε ($M^{-1}cm^{-1}$ or $Lmol^{-1}cm^{-1}$) is the absorbance unit, and D (10^{-4} esu^2 cm^2) is the dipole strength via the esu or electrostatic unit, which is a unit of charge in the cgs (centimeter-gram-second) system.

The maximum IR spectrum has been seen in the frequency range between 250 cm^{-1} and 3000 cm^{-1} by the peaks about 900 cm^{-1}, 1250 cm^{-1}, 1550 cm^{-1}, 1750 cm^{-1}, and 2250 cm^{-1}, respectively, for [(BNEJa) @ SWCNT] (Figure 6).

3.5. Frontier orbitals of HOMO & LUMO & UV-VIS spectroscopy.

The "highest occupied molecular orbital energy (HOMO)" and the "lowest unoccupied molecular orbital energy (LUMO)" have been calculated for the BP agent of (BNEJa) adsorbed onto (5,5) armchair SWCNT sensor in aqueous medium using CAM–B3LYP/6–311+G (d,p) (Table 3).

Table 3. The E_{HOMO} (a.u.), E_{LUMO} (a.u.), band energy gap (ΔE /eV), and other quantities (eV) for [(BNEJa) @ SWCNT] in aqueous medium using CAM–B3LYP/6–311+G (d,p).

Spin	μ	χ	η	E_{HOMO}	E_{LUMO}	ΔE
Singlet	–0.33	0.33	6.01	–0.23	0.21	12.02
Triplet	–6.48	6.48	0.14	–0.24	–0.23	0.28
Quintet	–6.64	6.64	0.02	–0.24	–0.24	0.04
Septet	–6.87	6.87	0.21	–0.26	–0.24	0.42
Nonet	–7.34	7.34	0.26	–0.28	–0.26	0.52
11-et	–7.62	7.62	0.02	–0.28	–0.28	0.05
13-et	–7.68	7.68	0.03	–0.28	–0.28	0.06
15-et	–7.86	7.86	0.14	–0.29	–0.28	0.28
17-et	–8.08	8.08	0.08	–0.30	–0.29	0.16
19-et	–8.23	8.23	0.08	–0.30	–0.30	0.17

The HOMO, LUMO, and band energy gap (eV) have indicated the pictorial explanation of the frontier molecular orbital, which are important factors for identifying the molecular characteristics of the drug delivery method through adsorbing the BP agent of (BNEJa), which has been surrounded by H_2O molecules on the (5,5) armchair SWCNT in aqueous medium (Table 3).

In other words, the HOMO shows the capability for giving an electron, while the LUMO, as an electron acceptor, exhibits the capability for accepting an electron. Therefore, the energy gap ($\Delta E = E_{LUMO} - E_{HOMO}$) indicates the energy difference between the frontier HOMO and LUMO orbitals, introducing the stability for the structure and unravels the chemical activity of the molecule (Table 3).

In this work, the energy gap has been established for the BP agent (BNEJa) interacting with SWCNT in an aqueous medium. Besides, frontier molecular orbitals play an important role in optical and electrical properties, as seen in UV–VIS spectra [33]. Moreover, to get more conclusive approval in identifying the compound characteristics of this structure, a series of chemical reactivity parameters consisting of chemical potential (μ), electronegativity (χ), and hardness (η) has been done (Table 3) [33]. The amounts of the parameters in Table 3 have exhibited a good stability of the BP agent through Langmuir adsorption on the SWCNT sensor.

4. Conclusions

To overcome this chronic disease, significant work has been done over decades, leading to various research efforts, different management techniques, and extensive use of nanotechnology. According to this research, NMR spectroscopy has suggested the positions of the active sites of labeled N, P, O, and F in the anti-diabetic drug (BNEJa) adsorbed onto the SWCNT sensor, which transfers the electron density of the polar bisphosphonate in the aqueous medium toward the carbon nanotube. Moreover, NQR characteristics for (BNEJa) @ SWCNT complex have represented the most fluctuation in the zone of the two phosphorus of PO_3 groups. The maximum IR spectrum for (BNEJa) @ SWCNT has been seen in the frequency range between 250–4500 cm^{-1} with the strongest peaks about 4100 cm^{-1}, 2250 cm^{-1}, 1750 cm^{-1}, 1550 cm^{-1}, 1250 cm^{-1}, and 900 cm^{-1}, respectively. Furthermore, the energy gap has indicated the energy difference between the frontier HOMO and LUMO orbitals, introducing the stability for (BNEJa) and discovering the chemical potential of (BNEJa) drug for the treatment of type 2 diabetes. The development of novel delivery systems for antidiabetic medications, including tablets and microstructures, is a focus of industry and numerous top research initiatives.

Author Contributions

Conceptualization, F.M.; methodology, F.M.; software, F.M.; validation, F.M. and M.M.; formal analysis, F.M. and M.M.; investigation, F.M. and M.M.; resources, F.M. and M.M.; data curation, F.M.; writing—original draft preparation, F.M.; writing—review and editing, M.M.; visualization, F.M. and M.M.; supervision, F.M.; project administration, F.M. All authors have read and agreed to the published version of the manuscript.

Institutional Review Board Statement

Not applicable.

Informed Consent Statement

Not applicable.

Data Availability Statement

Not applicable.

Funding

This research received no external funding.

Acknowledgments

In successfully completing this paper and its research, the authors are grateful to Kastamonu University.

Conflict of Interest

The author declares no conflict of interest.

References

1. Krause, M.; De Vito, G. Type 1 and Type 2 Diabetes Mellitus: Commonalities, Differences and the Importance of Exercise and Nutrition. *Nutrients* **2023**, *15*, 4279, https://doi.org/10.3390/nu15194279.
2. Cloete, L. Diabetes mellitus: an overview of the types, symptoms, complications and management. *Nurs. Stand. (1987)* **2021**, *37*, 61-66, https://doi.org/10.7748/ns.2021.e11709.
3. Genovese, M.; Imperatore, C.; Casertano, M.; Aiello, A.; Balestri, F.; Piazza, L.; Menna, M.; Del Corso, A.; Paoli, P. Dual Targeting of PTP1B and Aldose Reductase with Marine Drug Phosphoeleganin: A Promising Strategy for Treatment of Type 2 Diabetes. *Mar. Drugs* **2021**, *19*, 535, https://doi.org/10.3390/md19100535.
4. Kołodziej-Sobczak, D.; Sobczak, Ł.; Łączkowski, K.Z. Protein Tyrosine Phosphatase 1B (PTP1B): A Comprehensive Review of Its Role in Pathogenesis of Human Diseases. *Int. J. Mol. Sci.* **2024**, *25*, 7033, https://doi.org/10.3390/ijms25137033.
5. Song, J.; Lan, J.; Tang, J.; Luo, N. PTPN2 in the Immunity and Tumor Immunotherapy: A Concise Review. *Int. J. Mol. Sci.* **2022**, *23*, 1002, https://doi.org/10.3390/ijms231710025.
6. Baumgartner, C.K.; Ebrahimi-Nik, H.; Iracheta-Vellve, A.; Hamel, K.M.; Olander, K.E.; Davis, T.G.R.; McGuire, K.A.; Halvorsen, G.T.; Avila, O.I.; Patel, C.H.; Kim, S.Y.; Kammula, A.V.; Muscato, A.J.; Halliwill, K.; Geda, P.; Klinge, K.L.; Xiong, Z.; Duggan, R.; Mu, L.; Yeary, M.D.; Patti, J.C.; Balon, T.M.; Mathew, R.; Backus, C.; Kennedy, D.E.; Chen, A.; Longenecker, K.; Klahn, J.T.; Hrusch, C.L.; Krishnan, N.; Hutchins, C.W.; Dunning, J.P.; Bulic, M.; Tiwari, P.; Colvin, K.J.; Chuong, C.L.; Kohnle, I.C.; Rees, M.G.; Boghossian, A.; Ronan, M.; Roth, J.A.; Wu, M.-J.; Suermondt, J.S.M.T.; Knudsen, N.H.; Cheruiyot, C.K.; Sen, D.R.; Griffin, G.K.; Golub, T.R.; El-Bardeesy, N.; Decker, J.H.; Yang, Y.; Guffroy, M.; Fossey, S.; Trusk, P.; Sun, I.-M.; Liu, Y.; Qiu, W.; Sun, Q.; Paddock, M.N.; Farney, E.P.; Matulenko, M.A.; Beauregard, C.; Frost, J.M.; Yates, K.B.; Kym, P.R.; Manguso, R.T. The PTPN2/PTPN1 inhibitor ABBV-CLS-484 unleashes potent anti-tumour immunity. *Nature* **2023**, *622*, 850-862, https://doi.org/10.1038/s41586-023-06575-7.
7. Singh, J.P.; Li, Y.; Chen, Y.-Y.; Hsu, S.-T.D.; Page, R.; Peti, W.; Meng, T.-C. The catalytic activity of TCPTP is auto-regulated by its intrinsically disordered tail and activated by Integrin alpha-1. *Nat. Commun.* **2022**, *13*, 94, https://doi.org/10.1038/s41467-021-27633-6.
8. Lee, G.B.; Etherton-Beer, C.; Hosking, S.M.; Pasco, J.A.; Page, A.T. The patterns and implications of potentially suboptimal medicine regimens among older adults: a narrative review. *Ther. Adv. Drug Saf.* **2022**, *13*, 20420986221100117, https://doi.org/10.1177/20420986221100117.
9. Zhao, X.; An, X.; Yang, C.; Sun, W.; Ji, H.; Lian, F. The crucial role and mechanism of insulin resistance in metabolic disease. *Front. Endocrinol.* **2023**, *14*, 1149239, https://doi.org/10.3389/fendo.2023.1149239.

10. Rehan, F.; Zhang, M.; Fang, J.; Greish, K. Therapeutic Applications of Nanomedicine: Recent Developments and Future Perspectives. *Molecules* **2024**, *29*, 2073, https://doi.org/10.3390/molecules29092073.
11. Mollaamin, F. Computational Methods in the Drug Delivery of Carbon Nanocarriers onto Several Compounds in Sarraceniaceae Medicinal Plant as Monkeypox Therapy. *Computation* **2023**, *11*, 84, https://doi.org/10.3390/computation11040084.
12. Mollaamin, F.; Monajjemi, M. Carbon Nanotubes as Biosensors for Releasing Conjugated Bisphosphonates–Metal Ions in Bone Tissue: Targeted Drug Delivery through the DFT Method. *C* **2023**, *9*, 61, https://doi.org/10.3390/c9020061.
13. Mollaamin, F. Structural and Functional Characterization of Medicinal Plants as Selective Antibodies towards Therapy of COVID-19 Symptoms. *Antibodies* **2024**, *13*, 38, https://doi.org/10.3390/antib13020038.
14. Naumenko, E.; Guryanov, I.; Gomzikova, M. Drug Delivery Nano-Platforms for Advanced Cancer Therapy. *Sci. Pharm.* **2024**, *92*, 28, https://doi.org/10.3390/scipharm92020028.
15. Solorio-Rodriguez, S.A.; Williams, A.; Poulsen, S.S.; Knudsen, K.B.; Jensen, K.A.; Clausen, P.A.; Danielsen, P.H.; Wallin, H.; Vogel, U.; Halappanavar, S. Single-Walled vs. Multi-Walled Carbon Nanotubes: Influence of Physico-Chemical Properties on Toxicogenomics Responses in Mouse Lungs. *Nanomaterials* **2023**, *13*, 1059, https://doi.org/10.3390/nano13061059.
16. Fatima, M.; An, T.; Hong, K.-J. Revolutionizing mRNA Vaccines Through Innovative Formulation and Delivery Strategies. *Biomolecules* **2025**, *15*, 359, https://doi.org/10.3390/biom15030359.
17. Mollaamin, F.; Monajjemi, M. Application of DFT/TD-DFT Frameworks in the Drug Delivery Mechanism: Investigation of Chelated Bisphosphonate with Transition Metal Cations in Bone Treatment. *Chemistry* **2023**, *5*, 365-380, https://doi.org/10.3390/chemistry5010027.
18. Alshaaer, M.; Issa, K.; Alanazi, A.; Mallouh, S.A.; Afify, A.S.; Moustapha, M.E.; Komnitsas, K. Gradual Replacement of Ca^{2+} with Mg^{2+} Ions in Brushite for the Production of $Ca_{1-x}Mg_xHPO_4{\cdot}nH_2O$ Materials. *Minerals* **2021**, *11*, 284, https://doi.org/10.3390/min11030284.
19. Pabst, A.M.; Krüger, M.; Blatt, S.; Ziebart, T.; Rahimi-Nedjat, R.; Goetze, E.; Walter, C. Angiogenesis in the Development of Medication-Related Osteonecrosis of the Jaws: An Overview. *Dent. J.* **2017**, *5*, 2, https://doi.org/10.3390/dj5010002.
20. Lee, K.K.; Kim, H.; Lee, C.-S. Nitrogen-Containing Bisphosphonate Carbon Dots with High Affinity to Calcium-Based Biomaterials for Suppression of Osteoclasts. *BioChip J.* **2025**, *19*, 142–151, https://doi.org/10.1007/s13206-024-00189-5.
21. Frisch, M.J.; Trucks, G.W.; Schlegel, H.B.; Scuseria, G.E.; Robb, M.A.; Cheeseman, J.R.; Scalmani, G.; Barone, V.; Petersson, G.A.; Nakatsuji, H.; Li, X.; Caricato, M.; Marenich, A.V.; Bloino, J.; Janesko, B.G.; Gomperts, R.; Mennucci, B.; Hratchian, H.P.; Ortiz, J. V.; Izmaylov, A. F.; Sonnenberg, J.L.; Williams-Young, D.; Ding, F.; Lipparini, F.; Egidi, F.; Goings, J.; Peng, B.; Petrone, A.; Henderson, T.; Ranasinghe, D.; Zakrzewski, V.G.; Gao, J.; Rega, N.; Zheng, G.; Liang, W.; Hada, M.; Ehara, M.; Toyota, K.; Fukuda, R.; Hasegawa, J.; Ishida, M.; Nakajima, T.; Honda, Y.; Kitao, O.; Nakai, H.; Vreven, T.; Throssell, K.; Montgomery, J.A., Jr.; Peralta, J.E.; Ogliaro, F.; Bearpark, M.J.; Heyd, J.J.; Brothers, E.N.; Kudin, K.N.; Staroverov, V.N.; Keith, T.A.; Kobayashi, R.; Normand, J.; Raghavachari, K.; Rendell, A.P.; Burant, J.C.; Iyengar, S.S.; Tomasi, J.; Cossi, M.; Millam, J.M.; Klene, M.; Adamo, C.; Cammi, R.; Ochterski, J.W.; Martin, R.L.; Morokuma, K.; Farkas, O.; Foresman, J.B.; Fox, D.J. Gaussian 16, Revision C.01, Gaussian, Inc., Wallingford CT, **2016**.
22. Nagy, Á.; Schwarz, K. Special Issue "50th Anniversary of the Kohn–Sham Theory—Advances in Density Functional Theory". *Computation* **2016**, *4*, 45, https://doi.org/10.3390/computation4040045.
23. Mu, L.; Jiang, J.; Gao, S.; Li, X.-Y.; Sheng, S. A DFT Study of Band-Gap Tuning in 2D Black Phosphorus via Li^+, Na^+, Mg^{2+}, and Ca^{2+} Ions. *Int. J. Mol. Sci.* **2024**, *25*, 11841, https://doi.org/10.3390/ijms252111841.
24. Lee, C.; Yang, W.; Parr, R.G. Development of the Colle-Salvetti correlation-energy formula into a functional of the electron density. *Phys. Rev. B* **1988**, *37*, 785, https://doi.org/10.1103/PhysRevB.37.785.
25. Sahni, V. The Hohenberg-Kohn Theorems and Kohn-Sham Density Functional Theory. In Quantal Density Functional Theory; Sahni, V., Ed.; Springer Berlin Heidelberg: Berlin, Heidelberg, **2004**; pp. 99-123, https://doi.org/10.1007/978-3-662-09624-6_4.
26. Zois, K.P.; Tzeli, D. A Critical Look at Density Functional Theory in Chemistry: Untangling Its Strengths and Weaknesses. *Atoms* **2024**, *12*, 65, https://doi.org/10.3390/atoms12120065.
27. Mollaamin, F. Anchoring of 2D layered materials of $Ge_5Si_5O_{20}$ for (Li/Na/K)-(Rb/Cs) batteries towards Eco-friendly energy storage. *BMC Chem.* **2025**, *19*, 233, https://doi.org/10.1186/s13065-025-01593-0.

28. Zhou, J.; Doi, M. Derivation of Two-Fluid Model Based on Onsager Principle. *Entropy* **2022**, *24*, 716, https://doi.org/10.3390/e24050716.
29. Gerothanassis, I.P.; Kupka, T. New Insights into Nuclear Magnetic Resonance (NMR) Spectroscopy. *Molecules* **2025**, *30*, 1500, https://doi.org/10.3390/molecules30071500.
30. Monea, C.; Bizon, N. Nuclear Quadrupole Resonance Spectroscopy. In Signal Processing and Analysis Techniques for Nuclear Quadrupole Resonance Spectroscopy; Monea, C., Bizon, N., Eds.; Springer International Publishing: Cham, **2022**; pp. 17-31, https://doi.org/10.1007/978-3-030-87861-0_3.
31. Selmi, K.; Khalfallah, S.; Bouallegue, K. Modeling Electrical Potential in Multi-Dendritic Neurons Using Bessel Functions. *Med. Sci. Forum* **2024**, *28*, 2, https://doi.org/10.3390/msf2024028002.
32. Glendening, E.D.; Hiatt, D.M.; Weinhold, F. Natural Bond Orbital Analysis of Chemical Structure, Spectroscopy, and Reactivity: How it Works. In Comprehensive Computational Chemistry, 1st Edition; Yáñez, M., Boyd, R.J., Eds.; Elsevier: Oxford, **2024**; Volume 2, pp. 406-421, https://doi.org/10.1016/B978-0-12-821978-2.00077-5.
33. Abrosimov, R.; Moosmann, B. The HOMO-LUMO Gap as Discriminator of Biotic from Abiotic Chemistries. *Life* **2024**, *14*, 1330, https://doi.org/10.3390/life14101330.

Publisher's Note & Disclaimer